



## Article

# Combined Methodology for Rockfall Susceptibility Mapping Using UAV Imagery Data

Svetlana Gantimurova<sup>1,2</sup> and Alexander Parshin<sup>1,2,\*</sup>

<sup>1</sup> Siberian School of Geosciences, Irkutsk National Research Technical University, Lermontova St. 89, 664074 Irkutsk, Russia; lanagant@geo.istu.edu

<sup>2</sup> Vinogradov Institute of Geochemistry SB RAS, Favorsky St. 1A, 664033 Irkutsk, Russia

\* Correspondence: sarhin@geo.istu.edu; Tel.: +7-90-27-666-990

**Abstract:** Gravitational processes on cut slopes located close to infrastructure are a high concern in mountainous regions. There are many techniques for survey, assessment, and prognosis of hazardous exogenous geological processes. The given research describes using UAV data and GIS morphometric analysis for delineation of hazardous rockfall zones and 3D modelling to obtain an enhanced, detailed evaluation of slope characteristics. Besides the slope geomorphometric data, we integrated discontinuity layers, including rock plains orientation and fracture network density. Cloud Compare software 2.12 was utilised for facet extraction. Fracture discontinuity analysis was performed in QGIS using the Network GT plugin. The presented research uses an Analytical Hierarchy Process (AHP) to determine the weight of each contributing factor. GIS overlay of weighted factors is applied for rockfall susceptibility mapping. This integrated approach allows for a more comprehensive GIS-based rockfall susceptibility mapping by considering both the structural characteristics of the outcrop and the geomorphological features of the slope. By combining UAV data, GIS-based morphometric analysis, and discontinuity analysis, we are able to delineate hazardous rockfall zones effectively.

**Keywords:** UAV; rockfall; GIS; fracture analysis; facet extraction



**Citation:** Gantimurova, S.; Parshin, A. Combined Methodology for Rockfall Susceptibility Mapping Using UAV Imagery Data. *Remote Sens.* **2024**, *16*, 177. <https://doi.org/10.3390/rs16010177>

Academic Editors: Stephan van Gasselt and Shih-Yuan Lin

Received: 23 November 2023

Revised: 29 December 2023

Accepted: 30 December 2023

Published: 31 December 2023



**Copyright:** © 2023 by the authors. Licensee MDPI, Basel, Switzerland. This article is an open access article distributed under the terms and conditions of the Creative Commons Attribution (CC BY) license (<https://creativecommons.org/licenses/by/4.0/>).

## 1. Introduction

Rock failures pose a serious threat of damage to adjacent infrastructure. Unstable rock masses on slope cuts along roads and railroads are a matter of concern in mountainous geodynamically active regions [1–3]. Rockfalls are a common risk that frequently affect road systems, resulting in substantial financial loss [4–6]. Due to the complexity of the variables that cause landslides and the variety of sizes and shapes that landslides can take, mapping landslide susceptibility remains challenging [7].

The following rockfall triggering factors in recent thematic literature [8]: (i) climatic and weather conditions, including global climate change induced hydro-meteorological effects (i.e., alterations in temperature, moisture level, and precipitation rates); (ii) tectonic movements and seismic activity [9]; (iii) anthropogenic impact, deforestation and vegetation degradation. Contributing rockfall factors are certain conditions that influence rockfall susceptibility [10]. Generally, it is a combination of the geological, geomorphological, hydro-geological, and land cover properties of the territory. By examining the correlation between the aforementioned elements and actual rockfall incidents, numerous methods for locating rockfall sources have been suggested. Direct identification, morphometric techniques, spatially distributed techniques, and statistical techniques can be used to categorize these procedures [2].

Comprehensive analysis of the geomorphological situation and the identification of potentially hazardous areas are necessary to carry out preventive measures to mitigate the risk of rockfalls [6,11,12]. Slopes can be stabilized by a variety of techniques [13]. Mechanical engineering is frequently the method of choice, whether by fastening concrete

panels or blocks to a rock face, constructing barriers and protection structures, or removing soil from the top of slopes and moving it to the base to avoid undercutting. Additionally, slopes could also be pre-emptively cleared of unstable rocks that carry the danger of collapse [2]. Localization of hazardous zones is a primary task for slope management, as it reduces expenses of pedestrian surveys and observations in the field [14]. In addition, pedestrian surveys of such areas are unsafe, and therefore the development of methods for assessing the risks of rockfalls using Earth remote sensing technologies is a very urgent task. Also, remote sensing techniques significantly improve the regularity of observations, as well as evade some difficulties caused by limited accessibility [15,16].

There are a number of approaches for rockfall susceptibility and risk detection using remote sensing survey techniques [17]. However, there is no prevalent methodology providing the best modelling due to uncertainties in predicting hazardous exogenous geological processes and the diversity of contributing factors in particular conditions [18,19]. Researchers continue to compare the effectiveness of different methods and susceptibility models. Most of them calculate the morphometric characteristics of the slope from a digital surface model (DSM). Detailed DSM could be obtained from high-resolution remote sensing imagery data through photogrammetry, terrestrial laser scanning, or airborne laser scanning [13]. The quantity and quality of layers of rockfall factors calculated based on the DSM, as well as the degree of their correlation with the risks of hazardous processes, together determine the reliability of the hazard assessment. At the same time, each new scientifically substantiated factor makes it possible to increase this reliability, and therefore the development of means of remote data collection and the development of methods for their processing improve the quality of assessment and forecast, and represent a very relevant and practically significant task.

The authors' previous study resulted in a qualitative landslide susceptibility assessment of the study area using UAV multispectral imagery and photogrammetry techniques to get DSM [15]. As part of that study, a special survey technique using several camera angles, which minimized the loss of information on steep slopes, and a multispectral shooting mode, which expanded the capabilities of geomorphological interpretation. At that time, the final rockfall susceptibility map was compiled from only five main factors, but the potential of the data obtained allows us to calculate an additional number of informative rockfall hazard indicators. Thus, the high spatial and spectral resolution provided by the survey technique makes it possible to map subcentimeter objects even on steep slopes, which makes it possible to work with one of the most important signs of rockfalls—rock fracturing. Discontinuity extraction methods from products derived by LIDAR scanning, photogrammetry, or ground-based surveys provide valuable data that can be used to create detailed fracture networks for analysis [20–22]. These methods not only help identify potential failure zones, but also aid in determining the size and orientation of fractures and plains of the slope, enabling engineers to develop effective mitigation strategies.

GIS-based landslide susceptibility mapping for estimation areas where landslides may occur in the future is a well-researched approach and widely covered in articles [18,23,24]. Contributing factors are usually presented by altitude, slope, aspect, terrain ruggedness, other morphometric parameters, land cover, land use, lithology etc. [25]. The selection of these factors for susceptibility qualification is commonly based on expert opinion, the natural and technical conditions of the study area, and research objectives [8]. However, there is a lack of research on introducing the characteristics of the fracture network of the slope as a contributing factor when applying the GIS approach [26]. The geo-structural characteristics of discontinuities are crucial for slope stability analysis and rockfall event probability identification [27]. Thus, the novelty of the given research is to introduce factors of fracture density and facet orientation for GIS-based rockfall susceptibility mapping.

## 2. Study Site

The study site is located on the territory of the Irkutsk region in Russia (Figure 1a). The Circum-Baikal Railway is a part of the Trans-Siberian Railway. It is located in a mountainous

area, bordered by steep rocks on one side and limited by the shore of Lake Baikal on the other. Vehicle access is partially possible; there is no access by any other transport except for the rail, which runs back and forth once a day.

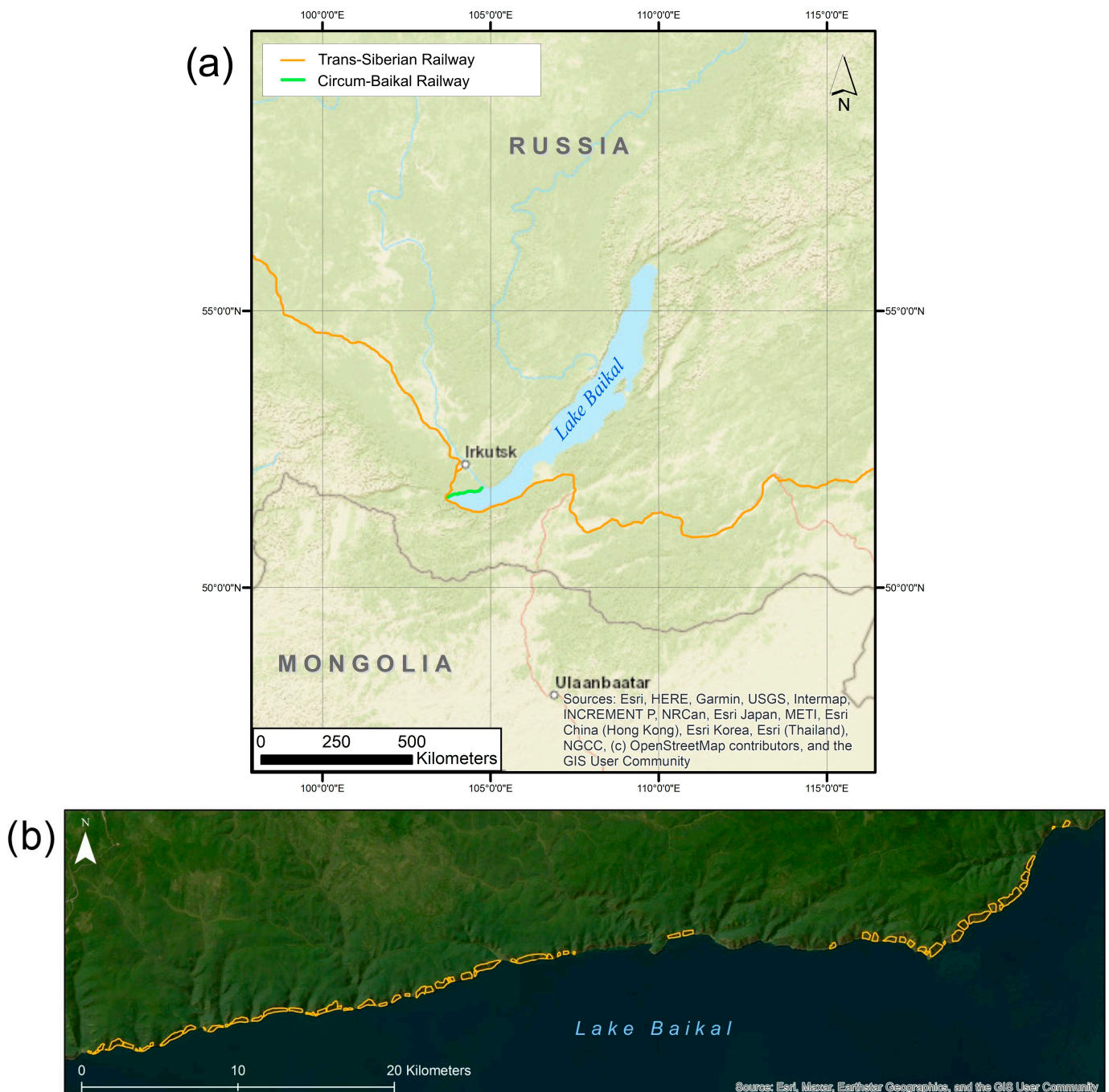


**Figure 1.** (a) Location of the Circum-Baikal Railway; (b) Location of the hazardous slopes along the Circum-Baikal Railway.

The Circum-Baikal Railway was built along the lakeshore in 1905; the section from the city of Slyudyanka to the village of Baikal is a unique monument of engineering art. The massive cutting of the steep slopes descending to the lake during the construction of the road provoked a catastrophic activation of geodynamic processes (Figure 2). In recent decades, the Circum-Baikal Road has been used exclusively for tourism purposes.



**Figure 2.** The photo of the tunnel entrance, railway and rocky slope.

Accessibility issues, severe climatic conditions, a large cover area, and administrative delays explain the deficient and sporadic observations. Monitoring systems require revision, enhancement, and elimination of data fragmentation.

### 2.1. Climate

The climate of the region is extremely continental. Summers are warm and humid, with significant rainfall. Winters are cold and dry. Winter lasts for 4–5 months. Between the third decade of November and the third decade of January, a stable snow cover forms. The height of the snow cover is 16–22 cm. The prevailing movement of air masses in winter is from northwest to southeast, and in summer from southeast to northwest. The average annual temperature is 1.5 °C below zero, and the average annual rainfall is 687 mm. Overall, the climate in this region is characterised by distinct seasons and a wide temperature range.

### 2.2. Geology

Basalts are overlain by eluvial-deluvial (on watersheds and their slopes) and alluvial (in valleys) Quaternary formations that play a part in the geological structure of the region. At the base of the upper part of the section, at a depth of tenths of a meter to 5 to 10 m or more, there is a stratum of basalts of various porosity, fissured, weathered, and of medium strength. The basalts are overlain by eluvial formations: gravel-gruss (with loamy-sandy aggregate 10 to 40%), gruss (with sandy-loamy aggregate from 5 to 35%, with the inclusion of crushed stone 20%), or large-block soils with loamy aggregate from five to 35%, exposed in the form of ruins on basalts in the most elevated areas. The thickness of the eluvial deposits ranges from 0.3 to 4.2 m. There are deluvial loams with a thicknesses of 0.25 to 4.6 m above, with the inclusion of gruss and crushed basalts ranging from 25 to 45%. Sometimes thicker than deluvial loams, there are interlayers of sandy loams and clays with the inclusion of crushed stone ranging from 15 to 45%. Their maximum thickness does not exceed 2.5 m. Boulder-pebble soils with silty filler or soft plastic loams with interlayers of silt and peat represent alluvial deposits developed in river valleys. The maximum thickness of alluvial deposits is 5 m.

### 2.3. Previous Studies

Since 1967, Russian Railways JSC has been recording rockfalls along the Circum-Baikal Railway. However, mainly large and noticeable collapses were recorded when stones fell on railway tracks or affected other infrastructure. Regular ground surveys of these areas proved impossible for economic reasons and due to the high risk to personnel [16]. In this regard, the Russian Railways JSC asked the authors to solve the problem of detailed survey and monitoring of 69 potentially hazardous slopes (Figure 1b) using UAVs and GIS technologies, and this gave us the material for this article.

### 3. Data

The objects of this study are highly steep slopes prone to rockfalls and scree, common in the territory within the boundaries from 72 km to 152 km of the Circum-Baikal Railway. The case study area shown in this paper is located at the 143rd km of the railway. The slope under consideration runs for 300 m along the rails. The inaccessibility of steep rocks can be overcome by using a UAV launched from the deck of a boat (Figure 3). The use of a UAV eliminates the need for personnel to physically access these hazardous areas.



**Figure 3.** Launching the UAS from the deck during data collection.

#### 3.1. UAV and GNSS Field Data Acquisition

To obtain the geospatial data necessary to create a DSM and calculate morphometric parameters related to the hazard of rockfalls and scree, the following equipment was used:

- (1) A SibGIS UAS (Unmanned Aerial System) hexacopter with an installed leg folding mechanism and two-axis camera gimbal. The weight of the UAV is 8 kg, including battery and propellers. This drone has 60 min of flying time, and 10 km remote control transmission distance.
- (2) The survey was undertaken using two 12 MP Mapir Survey 3 cameras—RGB and OCN (Red, Green, Blue, Orange (490 nm), Cyan (615 nm), NIR (808 nm)). The cameras were installed side by side on the same gimbal so that the distance between their lenses was no more than 4 cm. The camera shutters operated synchronously under external control from a PWM signal.

The survey was carried out using a previously developed method with two tilt angles at 45° and 90° [15]. The flight missions were prepared using the SibGIS Flight Planner intelligent module in such a way as to provide surveying of very rugged terrain with an approximately constant distance from the centre of photography to the slope, taking into account the camera tilt angle (target distance of 125 m), and an overlap no less, and often more than 80/80 percent between images. For radiometric calibration of images, compensating for changes in illumination during the day, Calibration Reflectance Target T3-R50 was used, as described in [15]. At this altitude, the resolution of the resulting images

is about 5.5 cm/pix. The take-off and landing of the UAV were carried out on the deck of a ship located a few tens or hundreds of meters from the shore, since landing on shore to install the RTK (Real Time Kinematic) base and launch the UAV would require separate approval from the Russian Railways security service for each of the 69 surveyed sites. Since it is impossible to install a RTK base on the rocking deck of a ship for working in RTK mode, which was previously used for high-precision image georeferencing, in this work the survey was carried out in PPK (Post-Processing Kinematics) mode. To synchronously control the camera shutters and record raw RINEX rover data on the UAV, a dual-frequency GNSS module Emlid Reach M2 was used, which allows surveying in PPK mode at a distance of up to 100 km from the base. Raw RINEX data from the Irkutsk station of the All-Eurasian service for providing differential correction data “CORPS” was used as base data.

### 3.2. Point Cloud Generation

For PPK processing of RINEX data from the rover and base and obtaining the precision coordinates of aerophotos, the open software product RTKLib was used.

After receiving the survey data, the photogrammetric processing of images was carried out using SfM-MVS photogrammetry in Agisoft PhotoScan [28]. The Structure-from-Motion (SfM) algorithm utilised various techniques, such as feature detection and matching, to establish correspondences between the images. These correspondences were then used to estimate the camera poses and triangulate the 3D points (Figure 4). The “high quality” setting ensured a more precise alignment of the images, while “reference preselection” helped in selecting reliable reference points for the alignment process [29]. As a result, a dense cloud of points was obtained, that is, a set of object surface vertices that are determined by the X, Y, and Z coordinates (Figure 5). The resulting point cloud and mesh were then visually inspected for accuracy and completeness. The inspection involved checking for any outliers or inconsistencies in the point cloud data. Additionally, the mesh was examined to ensure that it accurately represented the object’s surface topology and geometry. Next, a height map, a DSM, and an orthomosaic were built. Discontinuities can all be extracted using three-dimensional models that are generated from SfM [30].

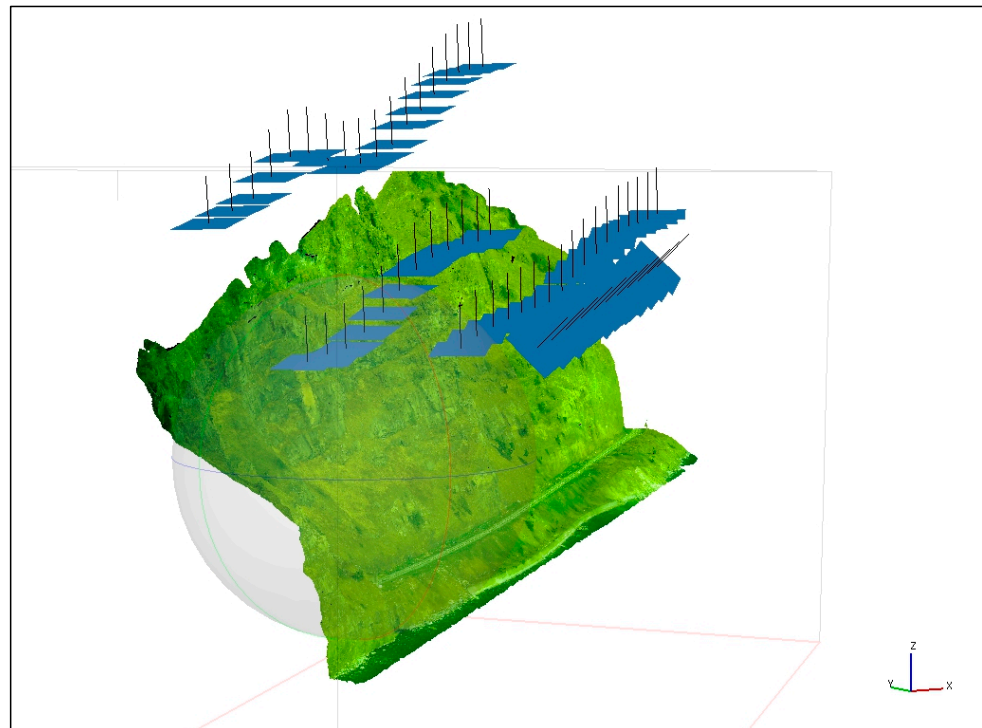


**Figure 4.** Camera positions and orientations.

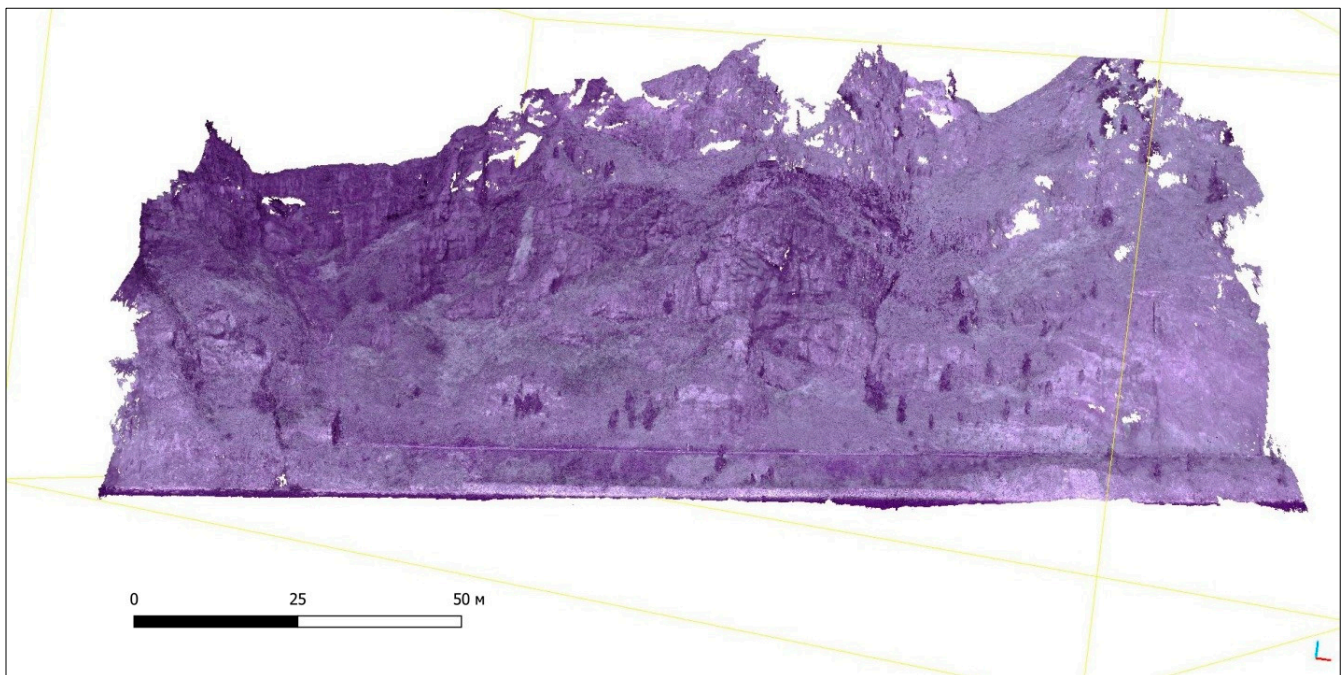


**Figure 5.** 3D point cloud of the rock slope.

#### 4. Methods

The objective of this research is to combine a geomorphometric approach, which derives parameters from DSM, fracture analysis, and overhanging rock identification using dense point cloud processing, with GIS for mapping potential rockfall sources. The proposed methodology consists of several steps (see Figure 6): (i) UAV data acquisition and imagery photogrammetry processing, (ii) facet extraction from the point cloud, (iii) fracture network extraction from images, (iv) slope morphometric analysis, and (v) GIS overlay and mapping the rockfall susceptibility on the 3D model of the rocky slope. Finally, in order to verify the accuracy of the rockfall susceptibility determination, a statistical and visual analysis based on the available field observation data was carried out. By utilizing UAV imagery and photogrammetry processing, a high-resolution 3D point cloud and DSM was generated, enabling accurate characterization of discontinuities and slope morphometric analysis. This information was then integrated into a GIS platform to create a map of rockfall susceptibility.

Our previous research resulted in a project of landslide susceptibility mapping using high resolution UAV data and GIS morphometric analysis [15]. The outcome of the research presented maps of potentially unstable rocks. The delineation of rockfall source areas was based on geomorphometric indices derived from the digital elevation model. The reliability of the method was approved by many other researchers [18,31–34]. Moreover, monitoring observations from past data acquisition supports the veracity of the obtained results. However, the technique can be improved by adding extra information describing slope stability, which is greatly impacted by discontinuities in the rock mass, including joints, faults, bedding planes, cleavage, lineation, foliation, and fractures. There may be mechanical discontinuities that are integral or incipient. When weathering occurs, intrinsic heterogeneities inside intact rock, known as integral discontinuities, can transform into mechanical discontinuities. In order to assess the characteristics of the rock mass and avoid engineering structure instability, discontinuities must be characterized [35,36].

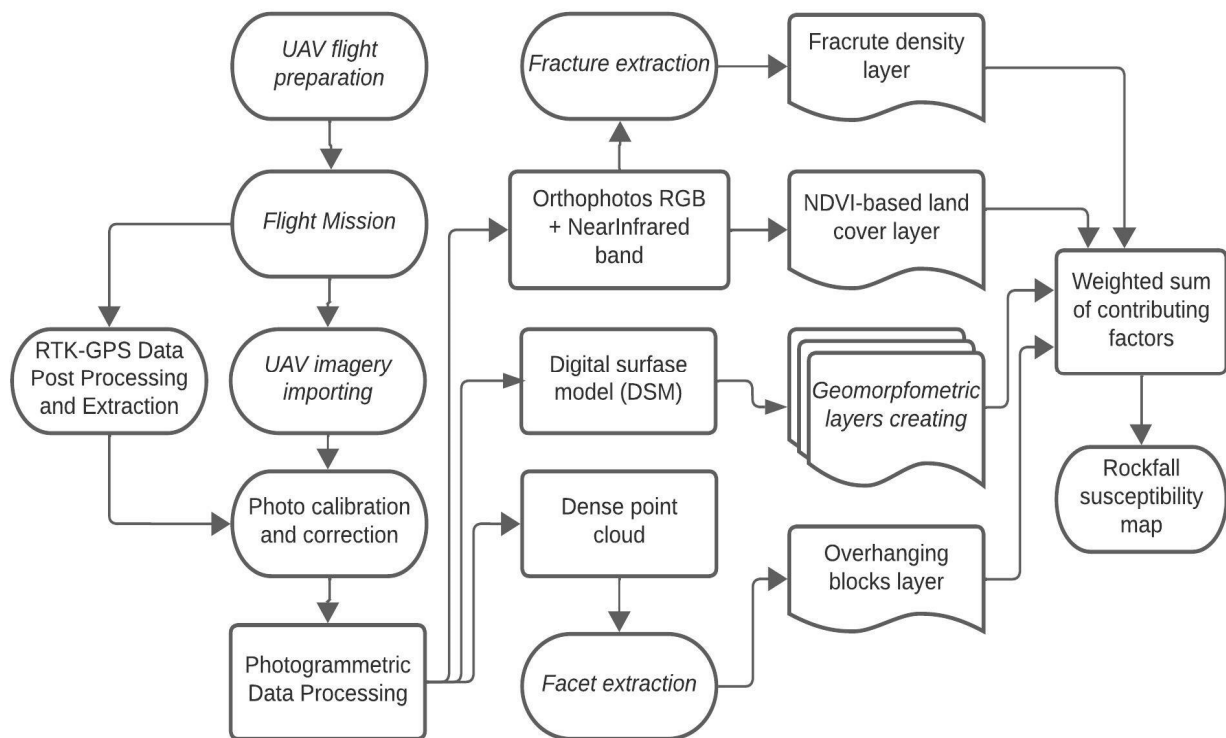


**Figure 6.** Technical flowchart.

#### 4.1. Geomorphometric Parameters

The slope topography, block shape, surface geology, and vegetation all play a role in the dynamics of rockfall [13]. These factors collectively determine the potential for rockfall occurrences and the trajectory of falling rocks. The following geomorphometric parameters were adopted to produce the rockfall susceptibility map: slope steepness, topographic wetness index, land cover, and profile curvature.

The angle of the slope plays a crucial role in determining the stability of rocks. As the slope angle increases, the gravitational force acting on the rocks intensifies, increasing their vulnerability to failure. Due to its close relationship to the forces at play, the slope angle can be used to directly connect slope movement. In particular, the slope's inclination affects the processes of erosion and infiltration brought on by surface runoff as well as the link between resistance and pressures in the subsurface [37].

Vegetation cover also plays an important role in the processes of erosion and infiltration. The presence of vegetation can help stabilize the soil, reducing the impact of surface runoff and promoting infiltration. Additionally, different types of vegetation can have varying effects on erosion rates, with some species providing more effective protection against erosion than others [38].

Erosion susceptibility can be determined by calculating the topographic wetness index [39]. It is a measure of the water saturation of the soil and can indicate areas that are more prone to erosion. This index takes into account factors such as slope, aspect, and the presence of depressions or valleys that may collect water. By calculating the topographic wetness index, land managers and scientists can identify areas that require specific erosion control measures to prevent further degradation of the terrain.

Profile curvature is another important factor that can be determined through topographic analysis. It measures the rate of slope surface changes in the direction of the slope or flow line and can provide valuable information about the stability of the land [40]. High positive values indicate convex slopes, which are more prone to erosion, while high negative values indicate concave slopes, which are more stable. By considering both the topographic wetness index and profile curvature, land managers can develop comprehensive erosion control strategies tailored to the specific characteristics of an area.

#### 4.2. Discontinuities Extraction Techniques

Slope failure phenomena are characteristic of steep mountain slopes, often composed of strongly fractured sedimentary, igneous, and metamorphic rocks. The fracture network is a highly causative factor for rockfalls as it serves as a pathway for groundwater and determines erodibility and slope failure mechanisms [41,42]. The modelling of fracture system parameters like distribution, connectivity, length, and angle is crucial in slope instability studies [43]. The choice of method for determining cracks as well as tracing is based on a compromise between the required accuracy and detail and the absence of determination errors and processing costs [41,43]. Manual techniques are reasonable when the size of the study site is relatively small or high accuracy is required, while using them on large areas is time-consuming and impractical [44,45]. Thiele et al. [46] compared the accuracy of manual fracture tracing, semi-automatic, and automatic techniques. Automated methods for extracting linear features in geosciences often use computer vision algorithms for edge and lineament detection [47]. However, these methods require fine-tuning and can detect false positives related to non-geological features. To improve objectivity and consistency, user-driven approaches have been developed, such as using an edge detection algorithm on orthophotos to optimize fracture traces and contacts. Automatic fracture tracing can be implemented using various programs and algorithms: GeoTrace plugin in QGIS [46], a MATLAB-based technique called the Discontinuity Set Extractor (DSE) [48,49], FracPaQ and ImageJ [35,50], and a Convolutional Neural Network (CNN)-based model named FraSegNet [51].

Nyberg et al. [52] analyses fracture networks using a two-dimensional areal sampling strategy. Network Geometry and Topology, an open-source ArcGIS toolbox was developed specifically for the quantitative geometric and topological analysis of fracture networks. The ArcGIS platform and NetworkGT plugin measure fracture length and strike directions based on traced segments. The fracture networks are described as spatial graphs with vertices and edges, with sinuosity approximated using piecewise linear edges. Automatic processing involves serial image processing steps like ridge ensemble computation, segmentation, skeletonization, and polyline fitting [45].

The Network GT plugin in QGIS is used in this study for fracture extraction. The binary grayscale photo of the slope is used as input for fracture extraction. The choice of thresholding is the first step in image segmentation, which is the process of dividing an image into different regions or objects. It helps in distinguishing different objects or features in an image based on their intensity values. By selecting the appropriate thresholding method, we can effectively separate foreground and background pixels, enhancing the accuracy of subsequent analysis or processing steps [52].

Edge-based image segmentation techniques do not allow identification of overhanging rocks, therefore 3-D point cloud processing stands a good stead. Automatic methods for analysing point cloud data have been proposed, using clustering or plane-fitting algorithms to segment and extract fracture or bedding faces [46]. However, the high computational cost of the automatic identification method presents a challenging issue [53]. Clustering analysis may be the most common method.

The facet detection plugin in CloudCompare was used in this study for automated identification and analysis of facets in 3D point cloud data [54,55]. In order to extract geological planes in rock outcrops from the dense point cloud, it was imported into CloudCompare 2.12. Forty-nine million points made up the slope that is being considered. Hough Normals computation was implemented first [56]. The Kd-Tree approach and Fast Marching approach are the two techniques suggested. While Fast Marching divides the cloud systematically into smaller patches, Kd-tree divides the 3D point cloud recursively into small planar patches. By categorizing meshes or facets according to orientation, a stereogram was created for the investigation of rock slope [50]. This plugin utilizes advanced algorithms to accurately detect and classify planes based on their size, shape, and orientation.

### 4.3. Susceptibility Mapping

GIS allows the application of a parameter map overlay to receive a susceptibility map, making it comparable in complexity and an effective method at local scale. However, the results are highly dependent on the correct selection of parameters for considering unique landscape conditions. Several multi-criteria evaluation techniques can be adopted for susceptibility assessment, such as the Analytical Hierarchy Process (AHP), logical regression model, frequency ratio model, and fuzzy logic [31]. The given study used the AHP model through pairwise comparison to determine the contribution of each factor to rockfall susceptibility. Table 1 represents pairwise comparison matrix, where  $W_i$  is the weight of each factor.

**Table 1.** The pairwise comparison matrix for LS factors: 1—equal importance, 2—weak importance, 3—moderate importance, 4—moderate plus, 5—strong importance.

AHP	Slope	TWI	Profile Curvature	Fracture Density	Land Cover	Overhanging Blocks	$W_i$
Slope	1	3	1	3	2	1	0.229
TWI	0.33	1	1	0.5	0.33	0.2	0.063
Profile curvature	1	1	1	0.5	0.25	0.25	0.091
Fracture density	0.33	2	2	1	0.33	0.33	0.101
Land cover	0.5	3	4	3	1	0.25	0.185
Overhanging blocks	1	5	4	3	4	1	0.332

The local morphometric terrain parameters are calculated in SAGA GIS. The slope tool creates a plane by fitting it to the elevation values of a  $3 \times 3$  cell neighbourhood surrounding the processing or centre cell. Therefore, we obtained a rate of maximum change in the z-value in degrees. TWI describes a cell's tendency to accumulate water, assumes steady-state conditions and spatially invariant conditions for infiltration and transmissivity, and highlights water runoff routes [39]. In the context of landslide susceptibility, profile curvature can help identify potential erosion or deposition areas within a landscape by indicating areas where flow and erosion processes are likely to be accelerated. A convex curvature suggests that water or sediment will be funnelled down slopes, increasing the likelihood of erosion. Conversely, a concave curvature indicates areas where sedimentation may occur as water and sediment collect in depressions or concave features [57]. Rockfall dynamics and resulting hazards are significantly impacted by the presence of trees along the slope, and thus land cover should be considered [58]. For vegetation cover characterization, the Normalized Difference Vegetation Index (NDVI) was used.

## 5. Results

### 5.1. Facet Extraction

The Fast Marching algorithm yielded faster processing and showed proper results (Figure 7). The point cloud was divided into smaller cells, which then computed basic planar objects and gradually aggregated them into polygons based on a planarity threshold. A tension parameter was used to modify the polygonal bounds surrounding segmented points. The location and direction of six of the primary families of discontinuities in the rocky massif may be determined using this semi-automatic method [59].

Fast Marching, compared to KD-tree, provided faster processing time, which made it a more efficient algorithm for certain applications, especially when handling massive amounts of data or needing quicker outcomes. The Fast Marching algorithm is particularly advantageous when dealing with problems that require real-time or near-real-time results. Additionally, its ability to handle dynamic environments and adapt to changing conditions further enhanced its superiority over the KD-tree algorithm.

The dominant discontinuity sets are green and blue. What we are interested in are dark-red planes that face downward on the slope and indicate overhanging blocks (Figure 8).

Overall, the mean dip/dip direction is  $039^{\circ}/145^{\circ}$  for the entire outcrop. By classifying facets based on their orientation, we can effectively pinpoint areas where overhanging blocks are present.

### 5.2. Fracture Extraction

The adaptive thresholding method was assessed as the most suitable for image segmentation in the given research. Then, the fracture network was digitized (Figure 9). After relieving of the result, short isolated features were cleaned, multiple intersections were removed, and deletion of circle and other artefacts was performed using a repair topology instrument.

Irregularities and vegetation shadows may be erroneously identified as fractures; in order to obtain adequate fracture density values when calculating density, a sampling area must be created, avoiding densely vegetated areas. This can be achieved by manually selecting a representative portion of the study area that is free from vegetation or any other potential sources of irregularities or by using NDVI for multispectral imaging. Additionally, it is important to carefully analyse and interpret the data collected from the sampling area to accurately determine fracture density and avoid any misinterpretations caused by false identification.

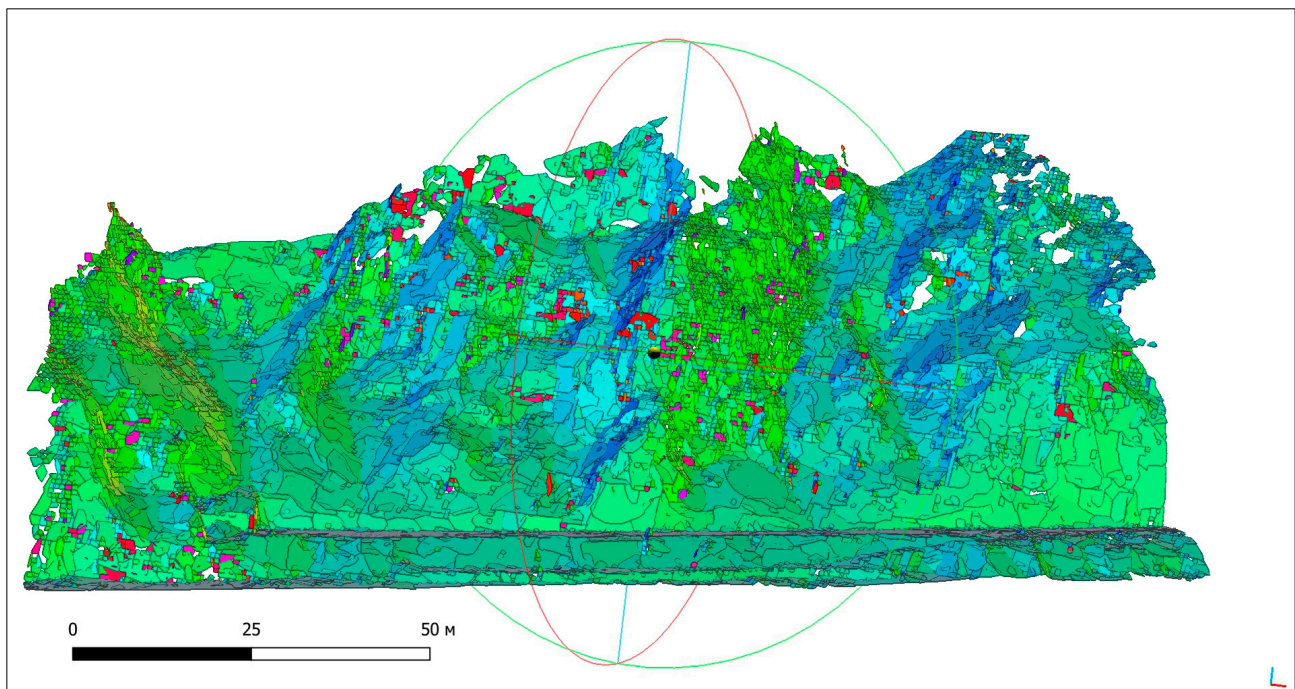


**Figure 7.** Results of automatic facets extraction (Fast Marching) from dense point cloud in Cloud Compare.

### 5.3. Rockfall Susceptibility Mapping

The main layers of features that were included in the final rockfall sustainability map are shown in the Figure 10.

The study used the AHP model to determine the contribution of each factor to rockfall susceptibility. The consistency ratio of each calculated parameter was less than 0.1, ensuring reliable weight determination. According to the pairwise comparison of contributing factors, the overhanging blocks layer had the greatest weight value (Table 1). This was done in order to determine these blocks even if the overall effect of other factors in these locations was modest. Steep slopes, areas without vegetation, and heavily fractured areas also had a high impact. Weighted parameters were overlaid for receiving the rockfall susceptibility map. The results show that rockfall susceptibility was classified into moderate- to high-susceptibility areas (Figure 11).

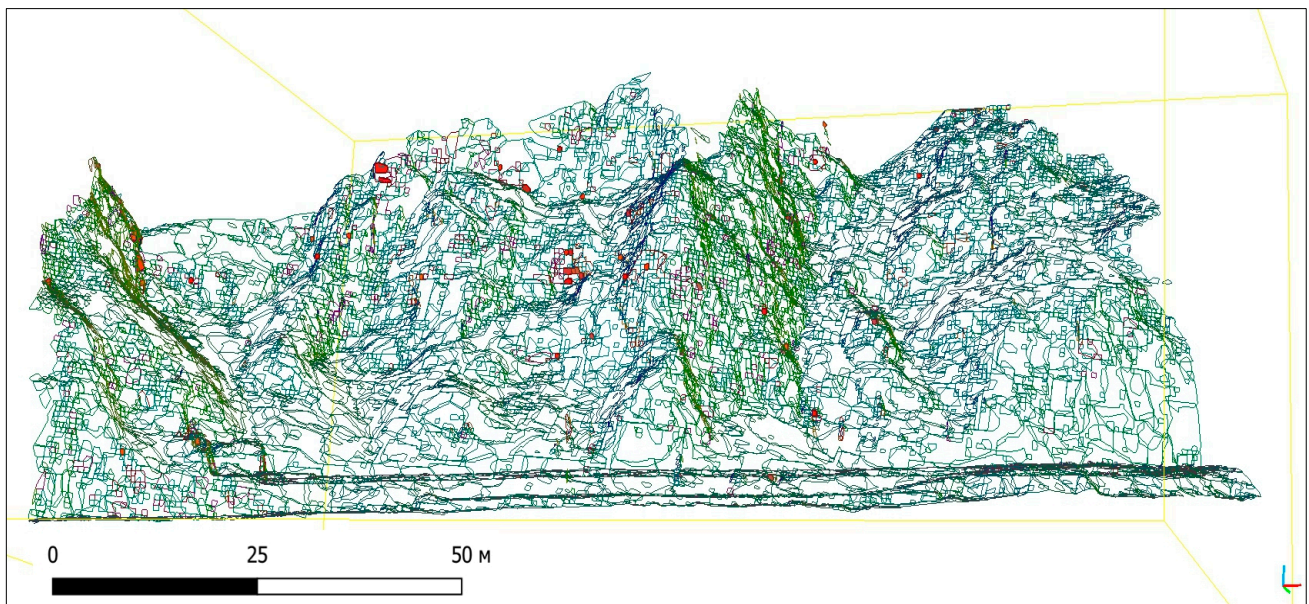


Figure 8. Front view of facet selection pinpointing overhanging blocks.

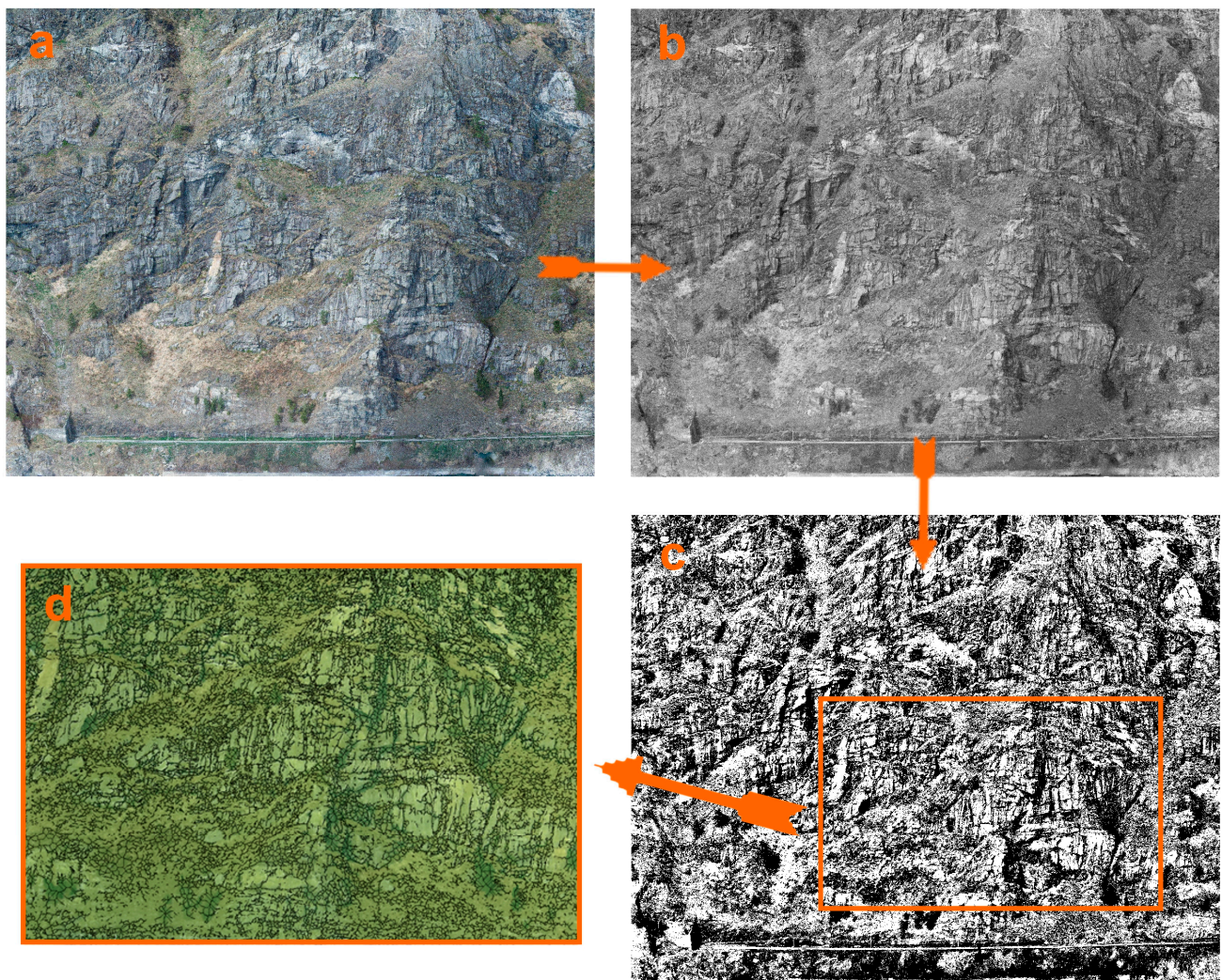


Figure 9. (a) RGB image of the slope; (b) Binary grayscale photo of the slope; (c) Adaptive thresholding results; (d) Digitalized fracture network.

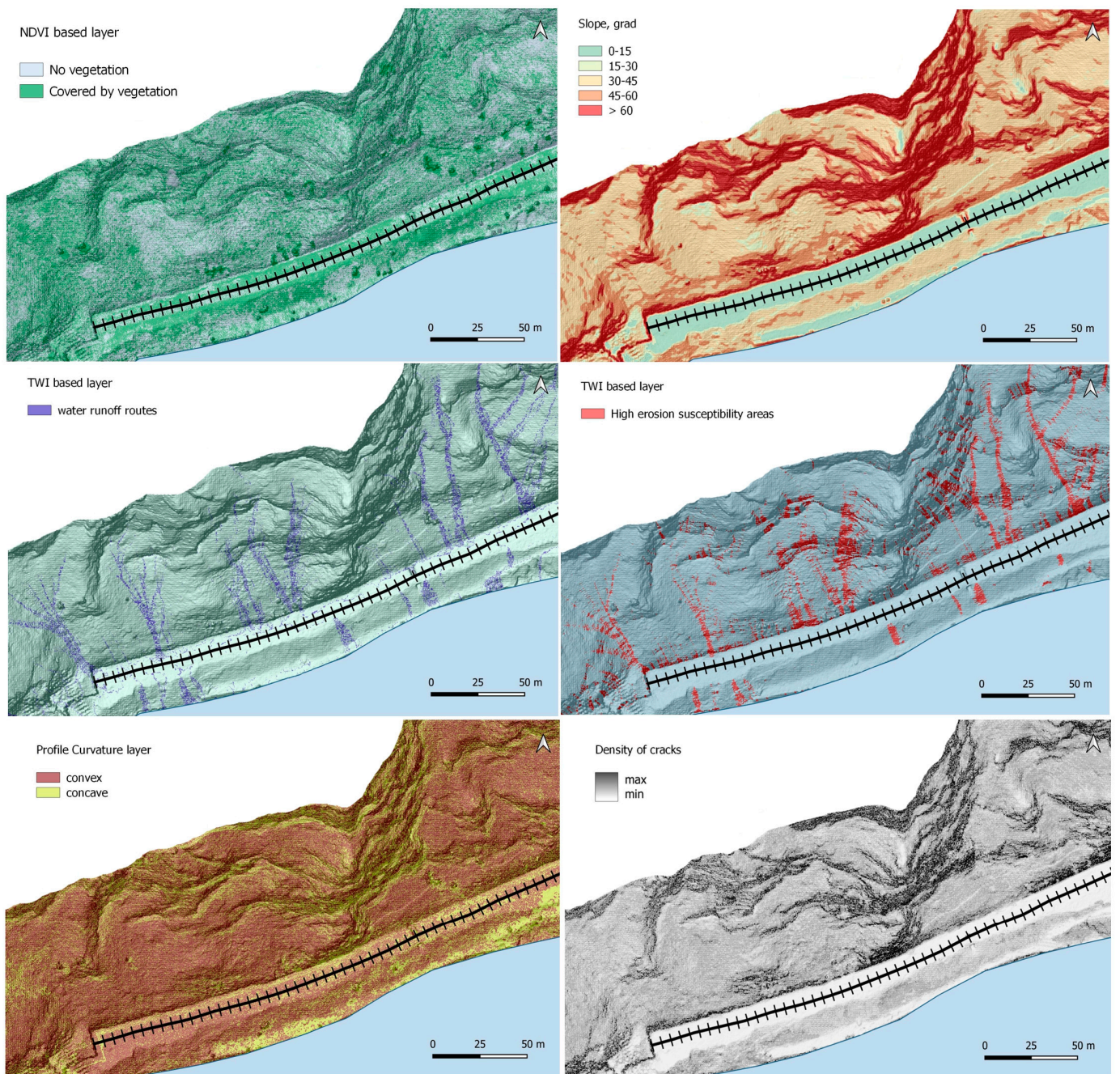


Figure 10. Main layers of features associated with the risk of rockfalls.

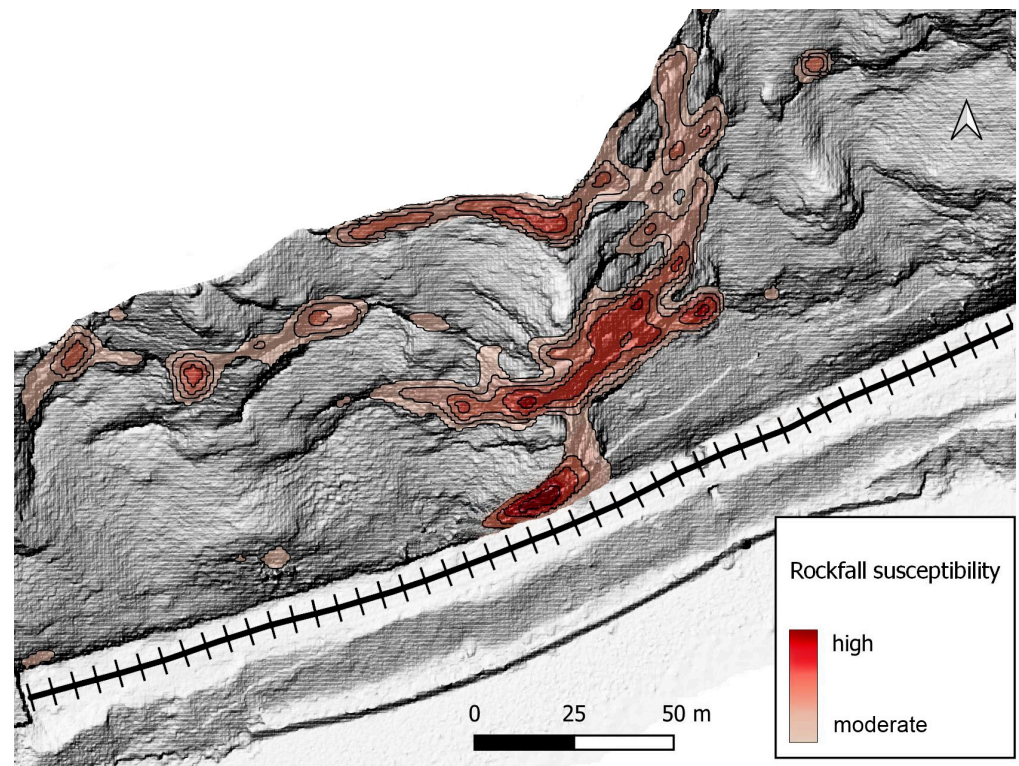


Figure 11. Rockfall susceptibility.

## 6. Discussion and Conclusions

For results validation, we compared susceptibility maps generated before introducing new factors and after. In addition, we verified the results to field observational information that was available.

In Figure 12, the green polygons are high rockfall susceptibility zones, modelled without counting the fracture density layer and the overhanging block layer. It can be seen that fewer zones were found. In both cases, large areas where the influences of all components coincided were delineated. However, smaller areas were not identified previously, although they pose a risk of collapse. According to available data, a crack meter is installed in the place marked in the Figure 12 at a height of 18 m and the block is extremely unstable. It became apparent that identifying this area as a hazardous zone was only possible with the addition of new parameters.

It also became possible to identify individual overhanging blocks (1–5 on Figure 12). The sufficiency of this finding was determined by visual comparison with a 3D model of the slope. Information about the number and location of overhanging blocks is necessary for planning work on clearing mountain slopes and installing rock barriers.

When the density of cracks on slopes was taken into consideration, the area of zones a, b, and c grew significantly. The field data indicates that the greatest threat to the path is represented by the rocky outcrops of the second and third tiers at an altitude of 40–60 m, which is zone “b” in Figure 12. The extent of this zone now matches the boundaries identified during on-site surveys. More accurate boundary and precise locations of hazardous zones are required for calculating areas of slopes and volumes of rock material that must be deliberately removed to prevent their collapse. Therefore, remote acquisition of such data is necessary for preliminary estimation of the cost of the work.

Discontinuities characteristics can be successfully used for enhancing rockfall susceptibility delineation. Extracted facets (plains oriented down the slope) designate overhanging blocks. Density of cracks of the outcrop was taken into account in calculations of the sum contribution of factors.

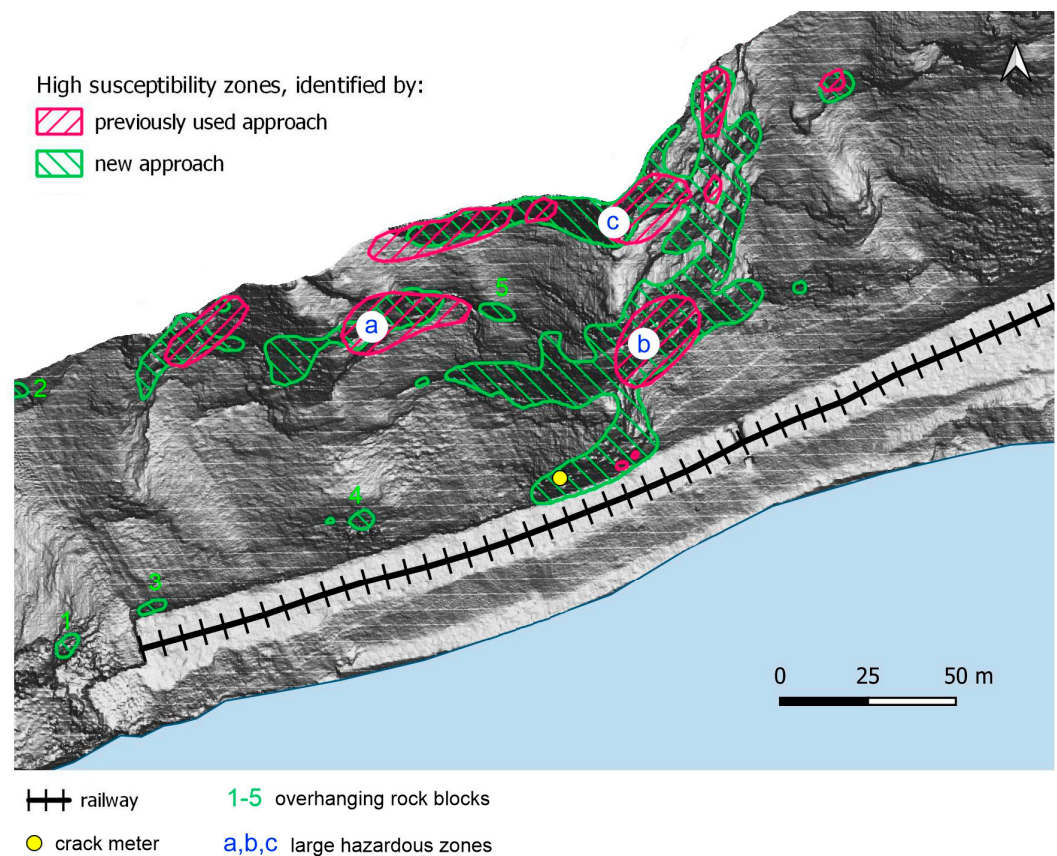


**Figure 12.** Rockfall susceptibility map of the slope excluding fracture density layer and overhanging blocks layer.

Evaluation of the effectiveness and accuracy of the suggested methodology can be improved by comparing the identified rockfall susceptibility zones with actual rockfall occurrences in the area. However, the scarcity of available statistical data does not allow us to conduct reliable statistical analysis. Field observations and measurements are limited due to Russian transport regulations, making it difficult to access protected slopes without authorization. Access to these lands is difficult even for Russian Railway workers and contractors, leading to rare field observations. Remote methods cannot be entirely identical to ground-based surveys. In this regard, the authors tried to maximize the quality of the final susceptibility models by including new informative features obtained from Earth remote sensing data, with all the objective limitations of this approach. The research was carried out as part of a practical project, one of the challenges was to develop a rapid approach, to optimize the time spent, and at the same time, increase the accuracy of localizing hazardous zones.

By adding more details about slope stability, the method can be enhanced even more. This additional information could include factors such as soil characteristics, weather conditions, and seismic activity [9]. By incorporating these variables into the analysis, a more comprehensive understanding of slope stability can be achieved. Additionally, considering the temporal aspect of slope stability, by analysing data from different time periods, it is possible to identify trends and patterns that can further enhance the accuracy of the method.

In the realm of geotechnical engineering and hazard assessment, the analysis of rockfall susceptibility plays a crucial role in ensuring the safety of infrastructure and human lives. The integration of multisensors, ground-based, and airborne-based data gathering methods can provide valuable functional data for simulating natural phenomena, validating models, and further developing them. This comprehensive approach allows

for a better understanding of slope dynamics and aids in the effective management of slope stability.

It should be noted that the rockfall susceptibility models obtained using the methodology described in this article for 69 sites of the Circum-Baikal Railway were important not just as additional scientific material, but for the first time in Russian practice, successfully passed examination as a standard result of engineering-geological surveys of slopes in order to select the most dangerous areas and calculations of the volume of work to eliminate hazards. Thus, the set of UAV and GIS technologies using the described methodology is now a legitimate replacement for slow and dangerous ground surveys, allowing us to obtain no less high-quality geotechnical reports in the form established by industry requirements using less time and money.

**Author Contributions:** Conceptualization and methodology, S.G. and A.P.; software, data acquisition, and pre-processing, S.G.; writing—original draft preparation, S.G.; writing—review and editing, A.P.; supervision, A.P. All authors have read and agreed to the published version of the manuscript.

**Funding:** This research was funded by Russian Ministry for Science and Education: Priority-2030.

**Data Availability Statement:** 3rd Party Data. Restrictions apply to the availability of these data due to the rules of the Russian Railways (the Circum-Baikal Railway is an object of cultural heritage and increased danger).

**Conflicts of Interest:** The authors declare no conflicts of interest. The funders had no role in the design of the study; in the collection, analyses, or interpretation of data; in the writing of the manuscript; or in the decision to publish the results.

## References

- Sharma, M.; Sharma, S.; Tripathi, G.; Singh, S.; Kanga, S.; Upadhyay, R. Geotechnical Stability Assessment of Road-Cut Slopes: A Case Study of Srinagar, Garhwal Himalaya, India. *Biol. Forum—Int. J.* **2023**, *15*, 1071–1080.
- Yan, J.; Chen, J.; Tan, C.; Zhang, Y.; Liu, Y.; Zhao, X.; Wang, Q. Rockfall Source Areas Identification at Local Scale by Integrating Discontinuity-Based Threshold Slope Angle and Rockfall Trajectory Analyses. *Eng. Geol.* **2023**, *313*, 106993. [\[CrossRef\]](#)
- Utlu, M.; ÖZTÜRK, M.; Şimşek, M. Evaluation of Rockfall Hazard Based on UAV Technology and 3D Rockfall Simulations. *Int. J. Environ. Geoinform.* **2021**, *10*, 1–16. [\[CrossRef\]](#)
- Guzzetti, F.; Paola, R.; Ghigi, S. Rockfall Hazard and Risk Assessment Along a Transportation Corridor in the Nera Valley, Central Italy. *Environ. Manag.* **2004**, *34*, 191–208. [\[CrossRef\]](#) [\[PubMed\]](#)
- Cignetti, M.; Godone, D.; Bertolo, D.; Paganone, M.; Thuegaz, P.; Giordan, D. Rockfall Susceptibility along the Regional Road Network of Aosta Valley Region (Northwestern Italy). *J. Maps* **2020**, *17*, 54–64. [\[CrossRef\]](#)
- Pokharel, B.; Lim, S.; Bhattarai, T.; Alvioli, M. Rockfall Susceptibility along Pasang Lhamu and Galchhi-Rasuwegadhi Highways, Rasuwa, Central Nepal. *Bull. Eng. Geol. Environ.* **2023**, *82*, 183. [\[CrossRef\]](#)
- Ghorbanzadeh, O.; Blaschke, T.; Gholamnia, K.; Meena, S.; Tiede, D.; Aryal, J. Evaluation of Different Machine Learning Methods and Deep-Learning Convolutional Neural Networks for Landslide Detection. *Remote Sens.* **2019**, *11*, 196. [\[CrossRef\]](#)
- Thomas, J.; Gupta, M.; Srivastava, P.; Petropoulos, G. Assessment of a Dynamic Physically Based Slope Stability Model to Evaluate Timing and Distribution of Rainfall-Induced Shallow Landslides. *ISPRS Int. J. Geo-Inf.* **2023**, *12*, 105. [\[CrossRef\]](#)
- Scuderi, L.; Onyango, E.; Nagle-McNaughton, T. A Remote Sensing and GIS Analysis of Rockfall Distributions from the 5 July 2019 Ridgecrest (MW7.1) and 24 June 2020 Owens Lake (MW5.8) Earthquakes. *Remote Sens.* **2023**, *15*, 1962. [\[CrossRef\]](#)
- Shano, L.; Raghuvanshi, T.; Meten, M. Landslide Susceptibility Evaluation and Hazard Zonation Techniques—A Review. *Geoenvironmental Disasters* **2020**, *7*, 18. [\[CrossRef\]](#)
- Amatya, P.M.; Kirschbaum, D.; Stanley, T.; Tanyas, H. Landslide Mapping Using Object-Based Image Analysis and Open Source Tools. *Eng. Geol.* **2021**, *282*, 106000. [\[CrossRef\]](#)
- Sinčić, M.; Bernat Gazibara, S.; Krkac, M.; Lukačić, H.; Mihalić Arbanas, S. The Use of High-Resolution Remote Sensing Data in Preparation of Input Data for Large-Scale Landslide Hazard Assessments. *Land* **2022**, *11*, 1360. [\[CrossRef\]](#)
- Fanos, A.; Pradhan, B. Laser Scanning Systems and Techniques in Rockfall Source Identification and Risk Assessment: A Critical Review. *Earth Syst. Environ.* **2018**, *2*, 163–182. [\[CrossRef\]](#)
- Mihalić Arbanas, S.; Bernat Gazibara, S.; Krkac, M.; Sinčić, M.; Lukačić, H.; Jagodnik, P.; Arbanas, Z. *Landslide Detection and Spatial Prediction: Application of Data and Information from Landslide Maps*; Springer: Cham, Switzerland, 2023; pp. 195–212, ISBN 978-3-031-18470-3.
- Gantimurova, S.; Parshin, A.; Erofeev, V. GIS-Based Landslide Susceptibility Mapping of the Circum-Baikal Railway in Russia Using UAV Data. *Remote Sens.* **2021**, *13*, 3629. [\[CrossRef\]](#)

16. Askarzadeh, T.; Bridgelall, R.; Tolliver, D. Systematic Literature Review of Drone Utility in Railway Condition Monitoring. *J. Transp. Eng. Part A Syst.* **2023**, *149*, 04023041. [CrossRef]
17. Albarelli, D.; Mavrouli, O.; Nyktas, P. Identification of Potential Rockfall Sources Using UAV-Derived Point Cloud. *Bull. Eng. Geol. Environ.* **2021**, *80*, 6539–6561. [CrossRef]
18. Hoa, P.; Tuan, N.Q.; Hồng, P.; Thao, G.; Binh, N. GIS-Based Modeling of Landslide Susceptibility Zonation by Integrating the Frequency Ratio and Objective–Subjective Weighting Approach: A Case Study in a Tropical Monsoon Climate Region. *Front. Environ. Sci.* **2023**, *11*, 635. [CrossRef]
19. Shiferaw, H. Study on the Influence of Slope Height and Angle on the Factor of Safety and Shape of Failure of Slopes Based on Strength Reduction Method of Analysis. *Beni-Suef Univ. J. Basic Appl. Sci.* **2021**, *10*, 31. [CrossRef]
20. Pagano, M.; Palma, B.; Ruocco, A.; Parise, M. Discontinuity Characterization of Rock Masses through Terrestrial Laser Scanner and Unmanned Aerial Vehicle Techniques Aimed at Slope Stability Assessment. *Appl. Sci.* **2020**, *10*, 2960. [CrossRef]
21. Matasci, B.; Stock, G.; Jaboyedoff, M.; Carrea, D.; Collins, B.; Guerin, A.; Matasci, G.; Ravelin, L. Assessing Rockfall Susceptibility in Steep and Overhanging Slopes Using Three-Dimensional Analysis of Failure Mechanisms. *Landslides* **2017**, *15*, 859–878. [CrossRef]
22. Millis, S.; Wong, D.; Chan, K. Digital Mapping of Discontinuities. In Proceedings of the 39th HKIE Geotechnical Division Annual Seminar, Hong Kong, China, 11 April 2019.
23. Tsachouridis, S.; Pavloudakis, F.; Pilalidis, K.; Myronidis, L.; Roumpos, C. Monitoring Slope Stability in Surface Mines: Are Low-Cost UAVs Used for Excavated Rock Volume Calculations Capable of Early Detection of Displacements? *MATEC Web Conf.* **2022**, *373*, 00052. [CrossRef]
24. Skilodimou, H.; Bathrellos, G.; Koskeridou, E.; Soukis, K.; Rozos, D. Physical and Anthropogenic Factors Related to Landslide Activity in the Northern Peloponnese, Greece. *Land* **2018**, *7*, 85. [CrossRef]
25. Nguyen Thi To, N.; Liu, C.-C. A New Approach Using AHP to Generate Landslide Susceptibility Maps in the Chen-Yu-Lan Watershed, Taiwan. *Sensors* **2019**, *19*, 505. [CrossRef] [PubMed]
26. Vanneschi, C.; Rindinella, A.; Salvini, R. Hazard Assessment of Rocky Slopes: An Integrated Photogrammetry–GIS Approach Including Fracture Density and Probability of Failure Data. *Remote Sens.* **2022**, *14*, 1438. [CrossRef]
27. Wang, W.; Zhao, W.; Chai, B.; Du, J.; Tang, L.; Yi, X. Discontinuity Interpretation and Identification of Potential Rockfalls for High-Steep Slopes Based on UAV Nap-of-the-Object Photogrammetry. *Comput. Geosci.* **2022**, *166*, 105191. [CrossRef]
28. AgiSoft PhotoScan Professional (Version 1.4.3) (Software). (2018). Available online: <http://www.agisoft.com/downloads/installer/> (accessed on 28 December 2023).
29. Kirsch, M.; Lorenz, S.; Zimmermann, R.; Andreani, L.; Tusa, L.; Pospiech, S.; Jackisch, R.; Khodadadzadeh, M.; Ghamisi, P.; Unger, G.; et al. Hyperspectral Outcrop Models for Palaeoseismic Studies. *Photogramm. Rec.* **2019**, *34*, 385–407. [CrossRef]
30. Donati, D.; Stead, D.; Onsel, E.; Mysiorek, J.; Chang, O. Remote Sensing and Geovisualization of Rock Slopes and Landslides. *Remote Sens.* **2023**, *15*, 3702. [CrossRef]
31. Asmare, D. Application and Validation of AHP and FR Methods for Landslide Susceptibility Mapping around Choke Mountain, Northwestern Ethiopia. *Sci. Afr.* **2022**, *19*, e01470. [CrossRef]
32. Psomiadis, E.; Papazachariou, A.; Soulis, K.; Alexiou, S.; Charalampopoulos, I. Landslide Mapping and Susceptibility Assessment Using Geospatial Analysis and Earth Observation Data. *Land* **2020**, *9*, 133. [CrossRef]
33. Pourghasemi, H.; Moradi, H.; Fatemi, S. Landslide Susceptibility Mapping by Binary Logistic Regression, Analytical Hierarchy Process, and Statistical Index Models and Assessment of Their Performances. *Nat. Hazard* **2013**, *69*, 749–779. [CrossRef]
34. Westen, C.J.; Rengers, N.; Soeters, R. Use of Geomorphological Information in Indirect Landslide Susceptibility Assessment. *Nat. Hazards* **2003**, *30*, 399–419. [CrossRef]
35. Shah, K.; Hashim, M.; Ariffin, K.S. Photogrammetry and Monte Carlo Simulation Based Statistical Characterization of Rock Mass Discontinuity Parameters. *Int. J. Min. Geo-Eng.* **2022**, *56*, 151–157. [CrossRef]
36. Hao, J.; Zhang, X.; Wang, C.; Wang, H.; Wang, H. Application of UAV Digital Photogrammetry in Geological Investigation and Stability Evaluation of High-Steep Mine Rock Slope. *Drones* **2023**, *7*, 198. [CrossRef]
37. Losasso, L.; Jaboyedoff, M.; Sdao, F. Potential Rock Fall Source Areas Identification and Rock Fall Propagation in the Province of Potenza Territory Using an Empirically Distributed Approach. *Landslides* **2017**, *14*, 1593–1602. [CrossRef]
38. Pooja, N.; Sangeetha, S. A Study on the Influence of Vegetation Growth on Slope Stability. *IOP Conf. Ser. Earth Environ. Sci.* **2022**, *1032*, 012003. [CrossRef]
39. Mattivi, P.; Franci, F.; Lambertini, A.; Bitelli, G. TWI Computation: A Comparison of Different Open Source GISs. *Open Geospat. Data Softw. Stand.* **2019**, *4*, 6. [CrossRef]
40. Peckham, S. Profile, Plan and Streamline Curvature: A Simple Derivation and Applications. *Proc. Geomorphometry* **2011**, *4*, 27–30.
41. Mammoliti, E.; Pepi, A.; Fronzi, D.; Morelli, S.; Volatili, T.; Tazioli, A.; Francioni, M. 3D Discrete Fracture Network Modelling from UAV Imagery Coupled with Tracer Tests to Assess Fracture Conductivity in an Unstable Rock Slope: Implications for Rockfall Phenomena. *Remote Sens.* **2023**, *15*, 1222. [CrossRef]
42. Palamakumbura, R.; Krabbendam, M.; Whitbread, K.; Arnhardt, C. A Review and Evaluation of the Methodology for Digitising 2D Fracture Networks and Topographic Lineaments in GIS. *Solid Earth Discuss.* **2019**, *2019*, 1–21.
43. Battulwar, R.; Zaré, M.; Emami, E.; Sattarvand, J. A State-of-the-Art Review of Automated Extraction of Rock Mass Discontinuity Characteristics Using Three-Dimensional Surface Models. *J. Rock Mech. Geotech. Eng.* **2021**, *13*, 920–936. [CrossRef]

44. Prabhakaran, R.; Urai, J.; Bertotti, G.; Weismüller, C.; Smeulders, D.M.J. Large-Scale Natural Fracture Network Patterns: Insights from Automated Mapping in the Lilstock (Bristol Channel) Limestone Outcrops. *J. Struct. Geol.* **2021**, *150*, 104405. [[CrossRef](#)]
45. Weismüller, C.; Prabhakaran, R.; Passchier, M.; Urai, J.; Bertotti, G.; Reicherter, K. Mapping the Fracture Network in the Lilstock Pavement, Bristol Channel, UK: Manual versus Automatic. *Solid Earth* **2020**, *11*, 1773–1802. [[CrossRef](#)]
46. Thiele, S.; Grose, L.; Samsu, A.; Micklethwaite, S.; Vollgger, S.; Cruden, A. Rapid, Semi-Automatic Fracture and Contact Mapping for Point Clouds, Images and Geophysical Data. *Solid Earth* **2017**, *8*, 1241–1253. [[CrossRef](#)]
47. Daghigh, H.; Tannant, D.; Daghigh, V.; Lichti, D.; Lindenbergh, R. A Critical Review of Discontinuity Plane Extraction from 3D Point Cloud Data of Rock Mass Surfaces. *Comput. Geosci.* **2022**, *169*, 105241. [[CrossRef](#)]
48. Riquelme, A.; Abellan, A.; Tomás, R.; Jaboyedoff, M. A New Approach for Semi-Automatic Rock Mass Joints Recognition from 3D Point Clouds. *Comput. Geosci.* **2014**, *68*, 38–52. [[CrossRef](#)]
49. Robiati, C.; Mastrantonio, G.; Francioni, M.; Eyre, M.; Coggan, J.; Mazzanti, P. Contribution of High-Resolution Virtual Outcrop Models for the Definition of Rockfall Activity and Associated Hazard Modelling. *Land* **2023**, *12*, 191. [[CrossRef](#)]
50. Healy, D.; Rizzo, R.; Cornwell, D.; Farrell, N.; Watkins, H.; Timms, N.; Gomez-Rivas, E.; Smith, M. FracPaQ: A MATLAB™ Toolbox for the Quantification of Fracture Patterns. *J. Struct. Geol.* **2016**, *95*, 1–16. [[CrossRef](#)]
51. Chen, J.; Zhou, M.; Huang, H.; Zhang, D.; Peng, Z. Automated Extraction and Evaluation of Fracture Trace Maps from Rock Tunnel Face Images via Deep Learning. *Int. J. Rock Mech. Min. Sci.* **2021**, *142*, 104745. [[CrossRef](#)]
52. Nyberg, B.; Nixon, C.; Sanderson, D. NetworkGT: A GIS Tool for Geometric and Topological Analysis of Two-Dimensional Fracture Networks. *Geosphere* **2018**, *14*, 1618–1634. [[CrossRef](#)]
53. Fu, H.; Chen, W.; Fu, J. Chapter 4—Potential Hazard Prediction of Rockfalls. In *Rock Mechanics and Engineering*; Fu, H., Chen, W., Fu, J., Eds.; Elsevier: Amsterdam, The Netherlands, 2021; pp. 127–137. ISBN 978-0-12-822424-3.
54. Tung, W.; Nagendran, S.; Mohamad Ismail, M.A. 3D Rock Slope Data Acquisition by Photogrammetry Approach and Extraction of Geological Planes Using FACET Plugin in CloudCompare. *IOP Conf. Ser. Earth Environ. Sci.* **2018**, *169*, 012051. [[CrossRef](#)]
55. Dewez, T.; Girardeau-Montaut, D.; Allanic, C.; Rohmer, J. Facets: A cloudcompare plugin to extract geological planes from unstructured 3d point clouds. *ISPRS—Int. Arch. Photogramm. Remote Sens. Spat. Inf. Sci.* **2016**, *XLI-B5*, 799–804. [[CrossRef](#)]
56. Boulch, A.; Marlet, R. Fast and Robust Normal Estimation for Point Clouds with Sharp Features. *Comput. Graph. Forum* **2012**, *31*, 1765–1774. [[CrossRef](#)]
57. Buitrago Escobar, J.; Martinez, J. Digital Elevation Models (DEM) Used to Assess Soil Erosion Risks: A Case Study in Boyaca, Colombia. *Agron. Colomb.* **2016**, *34*, 239–249. [[CrossRef](#)]
58. Lanfranconi, C.; Frattini, P.; Sala, G.; Bertolo, D.; Sun, J.; Crosta, G. Accounting for the Effect of Forest and Fragmentation in Probabilistic Rockfall Hazard. *Nat. Hazards Earth Syst. Sci.* **2023**, *23*, 2349–2363. [[CrossRef](#)]
59. Gallo, I.; Martinez-Corbella, M.; Sarro, R.; Iovine, G.; Lopez Vinielles, J.; Hernández Ruiz, M.; Robustelli, G.; Mateos, R.; López-Davalillo, J.C. An Integration of UAV-Based Photogrammetry and 3D Modelling for Rockfall Hazard Assessment: The Cárcavos Case in 2018 (Spain). *Remote Sens.* **2021**, *13*, 3450. [[CrossRef](#)]

**Disclaimer/Publisher’s Note:** The statements, opinions and data contained in all publications are solely those of the individual author(s) and contributor(s) and not of MDPI and/or the editor(s). MDPI and/or the editor(s) disclaim responsibility for any injury to people or property resulting from any ideas, methods, instructions or products referred to in the content.